THE ASTROPHYSICAL JOURNAL, 526:854–861, 1999 December 1

OPTICAL AND INFRARED OBSERVATIONS OF THE BIPOLAR PROTO–PLANETARY NEBULA HENIZE 401[1]

PEDRO GARCÍA–LARIO
ISO Data Centre, Estación de Seguimiento de Satélites de Villafranca del Castillo, Apartado de Correos 50727, E-28080 Madrid, Spain

ANGELS RIERA
Departament de Física i Enginyeria Nuclear, Universitat Politècnica de Catalunya, Avenida Víctor Balaguer s/n, E-08800 Vilanova i la Geltrú, Spain; and Departament d'Astronomia i Meteorologia, Universitat de Barcelona, Avenida Diagonal 647, E-08028 Barcelona, Spain

AND

ARTURO MANCHADO
Instituto de Astrofísica de Canarias, E-38200 La Laguna, Tenerife, Spain
Received 1998 December 4; accepted 1999 July 16

ABSTRACT

Based on optical and near-infrared ground-based spectroscopy and optical and near-infrared *Hubble Space Telescope* (*HST*) images, we confirm the classification of Hen 401 as a bipolar proto–planetary nebula. *HST* images reveal a highly elongated morphology, consisting of two main bipolar lobes of unequal surface brightness separated by a dark lane of dust with a total extension of $28'' \times 3''$, superimposed on a much fainter background emission of elliptical shape extending over $\sim 10'' \times 5''$. The simultaneous detection of spectral lines formed under very different density conditions, together with the strong obscuration observed along the equatorial plane, is interpreted as the signature of a circumstellar disk, which would be responsible for the strong collimation observed. We conclude that the emission observed is mainly due to scattering of the light originated in the fluorescence-excited inner region of the circumstellar disk. In addition, we also report the detection of strong molecular H_2 emission in the near infrared, confirming that the onset of the H_2 emission occurs in proto–PNs after the bipolar structure has developed, but before photoionization takes place.

Subject headings: circumstellar matter — infrared: ISM: continuum — planetary nebulae: individual (Henize 401)

1. INTRODUCTION

Henize 3-401 (= IRAS 10178−5958, hereafter Hen 401) was first identified as a star in the transition phase between the asymptotic giant branch (AGB) and the planetary nebula (PN) stages by Parthasarathy & Pottasch (1989) on the basis of its far-infrared *IRAS* colors. This object was previously cataloged in the list of Cool Carbon Stars compiled by Stephenson (1971) with the number 1662 (probably a misidentification), and later as a Be star by Sanduleak & Stephenson (1973) on the basis of its low-dispersion optical spectrum. Allen & Glass (1975) identified the object as an emission-line star with infrared dust emission, and Allen (1978) reported the detection of an extended bipolar reflection nebula around a B-type central star and the presence of permitted and forbidden emission lines of singly ionized iron in the optical spectrum, as well as other low-excitation forbidden emission lines and strong Balmer emission. Scarrot & Scarrot (1995) suggest from polarization measurements that the circular polarization pattern found is consistent with the presence of a circumstellar disk, which might be responsible for collimating the outflow.

Hen 401 was not detected in the OH maser emission line at 1612 MHz by Silva et al. (1993), but it was detected in CO at millimeter wavelengths by Loup et al. (1990) and by Bujarrabal & Bachiller (1991), suggesting a C-rich nature of the outer envelope. The CO lines detected are weak, probably due to an efficient photodissociation of this molecule by the UV radiation coming from the central star, and broad, corresponding to an expansion velocity of the circumstellar envelope of 16 km s^{-1}.

Recently, García-Lario et al. (1997) confirmed the detection of a strong near-infrared excess toward this source, which was interpreted as the signature of large amounts of hot dust in the circumstellar envelope, resulting from recent mass loss. Based on the overall emission of Hen 401 in the infrared from 1 to 100 μm, they concluded that the *IRAS* source should be classified as a PN in a very early evolutionary stage or as a proto-PN.

In this paper we confirm this classification and show deep optical and near-infrared images taken with the *Hubble Space Telescope* (*HST*), which reveal a highly collimated bipolar morphology. A detailed analysis of the low-resolution optical spectrum is also carried out. In addition, we report the detection of strong H_2 molecular emission in the near infrared. This adds another member to the short list of four proto-PNs that have been found to show H_2 emission so far (Weintraub et al. 1998).

2. OBSERVATIONS

Low-resolution long-slit optical spectra were taken at the 1.52 m ESO telescope (La Silla, Chile). The Boller & Chivens spectrograph was used at two different epochs, in 1990 February and 1995 February, with a CCD as detector attached to the Cassegrain focus of this telescope. In 1990 February, the spectral range 4040–6940 Å was covered with a spectral resolution of 2.8 Å $pixel^{-1}$, while in 1995 Feb-

[1] Based on observations collected at the European Southern Observatory (La Silla, Chile) and observations made with the NASA/ESA *Hubble Space Telescope*, obtained from the data archive at the Space Telescope Science Institute, which is operated by the Association of Universities for Research in Astronomy, Inc., under NASA contract NAS 5-26555.

ruary we covered the range 3500–11200 Å, with a spectral resolution of 3.8 Å pixel^{-1}. The slit width was 1".6 at both epochs. The slit was always oriented along the bipolar axis and through the central star. Several exposures were taken, with different integration times, up to a maximum of 1800 s.

Near-infrared spectra were also taken at La Silla using the infrared spectrograph IRSPEC attached to the Nasmyth focus of the 3.5 m NTT telescope during observations carried out in 1993 March. Spectra were centered at 2.122 and 2.166 μm, wavelengths corresponding to the $1 \rightarrow 0$ $S(1)$ vibrational-rotational emission line of molecular hydrogen, H_2, and H I Brγ, respectively with the slit again aligned along the bipolar axis of the nebula and through the central star. This time the slit width was 4".5. The standard beam-switching technique was used in order to subtract the sky background. IRSPEC is a cryogenically cooled grating spectrometer equipped with a 58×62 pixel InSb array, which provides a resolving power of around 2000 at the observed wavelengths.

The data-reduction process includes bias and flat-field corrections, as well as wavelength calibration, sky subtraction, and absolute flux calibration using comparison standard stars for both optical and near-infrared spectroscopic observations.

High spatial resolution optical (0".045 pixel^{-1}) and near-infrared (0".075 pixel^{-1}) images of Hen 401 were retrieved from the *HST* Data Archive. A detailed description of these images can be found in a recent paper by Sahai, Bujarrabal, & Zijlstra (1999). They were originally obtained as part of proposals 6816 (optical data; PI, R. Sahai) and 7840 (near-infrared data; PI, S. Kwok). Optical images with exposure times ranging from 200 to 600 s were obtained on 1997 June 12 using the Wide Field Planetary Camera 2 (WFPC2) in the light of Hα and the [S II] doublet 6717, 6731 Å through the narrow F656N and F673N filters, respectively, and in the continuum through the broad F606W filter centered around 6060 Å. Near-infrared images were obtained using NICMOS on board *HST* on 1998 March 6 in the light of H_2 2.122 μm and in the adjacent continuum at 2.149 μm through the narrow F212N and F215N filters, with exposure times slightly below 300 s in all cases. Cosmic-ray hits were eliminated from individual images. After this, and for each filter, all the available images were recentered and combined into a single image in order to increase the signal-to-noise ratio.

3. RESULTS

3.1. *HST Imaging*

HST images of Hen 401 (see Fig. 1) reveal a spectacular highly elongated structure consisting of two main bipolar lobes of unequal surface brightness extending over $28'' \times 3''$, separated by a dark lane of dust. The major axis is oriented along a position angle of 73°. The intensity ratio of the maximum peaks of the two lobes is $\simeq 3.5$ (southwest/northeast) in the optical range, while the contrast is not so strong in the near-infrared, where the same ratio drops to ~ 2. Assuming axial symmetry, the different brightness observed suggests shading of the northeast lobe by an equatorial disk of dust. The central star is detected very faintly in the optical images and appears much brighter in the near-infrared, which is consistent with a very strong reddening.

The *HST* images reveal a clumpy structure in the outermost nebular regions. In addition, the main bipolar lobes appear to be superimposed on a central faint emission with a more elliptical shape extending over $\sim 10'' \times 5''$, probably the remnant of the circumstellar shell previously ejected during the AGB phase.

Figure 1 shows logarithmic-scale images of Hen 401 taken in the light of Hα and the optical continuum around 6000 Å. They look very similar, and are also identical to the images obtained in other filters not shown in this figure. This suggests that the illuminated lobes emit as a consequence of dust scattering and are not yet photoionized.

The same figure (Fig. 1, *bottom*) also shows the logarithmic-scale H_2 continuum-subtracted image of Hen 401 at 2.122 μm (*left*), together with the image containing the emission in the adjacent continuum at 2.15 μm (*right*). In order to obtain the continuum-subtracted image, the adjacent continuum image was subtracted from the H_2 image after rescaling the continuum image by the appropriate factor using other stars in the field. While the continuum image looks very similar to the optical images, as expected if most of the emission is due to dust scattering, the H_2 continuum-subtracted image shows that there is intrinsic H_2 emission, coming mainly from the walls of the lobes. Unfortunately, the central part is dominated by noise caused by the subtraction of the bright central star, and therefore it is not possible to know whether or not H_2 emission is present in the central region of Hen 401.

3.2. *Near-Infrared Spectroscopy*

The near-infrared spectrum reveals a strong H_2 $1 \rightarrow 0$ $S(1)$ emission at 2.122 μm, which constitutes a new detection. This emission is 1.75 ± 0.10 times brighter than Brγ, which is also detected in emission. The ratio H_2/Br$\gamma \sim 1.75$ is similar to the values found in other very young PNs, although much higher ratios (H_2/Br$\gamma \geq 10$) are sometimes observed in more evolved H_2-dominated bipolar PNs (Guerrero et al. 1999).

So far, only a handful of objects in this short transition phase are known to show H_2 emission (Weintraub et al. 1998). Usually, this emission is interpreted as the signature of shock-excited gas in the circumstellar envelopes of these stars, but fluorescence might also play an important role in the origin of the emission observed.

The integrated fluxes of the H_2 2.122 μm and Brγ 2.166 μm lines are 7.63×10^{-12} ergs s^{-1} cm^{-2} and 4.36×10^{-12} ergs s^{-1} cm^{-2}, respectively, with an estimated uncertainty of 10%. They are not corrected for extinction.

3.3. *Optical Spectroscopy*

Hen 401 shows a rich emission-line optical spectrum (see Fig. 2) characterized by the presence of strong and broad H I Balmer lines over a faint and reddened continuum, together with permitted emission lines of He I, Fe II, O I, and the infrared Ca II triplet (see Fig. 3), as well as forbidden emission lines of [Fe II], [N II], [O I], [S II], and [Ca II]. Within the uncertainties, no variability has been found in the optical spectra taken in 1990 and 1995, and both of them also look very similar to the spectrum published by Allen (1978). The extended spectrum does not show significant differences between the inner central region and the lobes.

Line identifications are given in Table 1. The identified transitions are denoted by their ionic species, followed by their Moore (1972) multiplet number in parentheses. More than one transition is listed in the case of blends or when

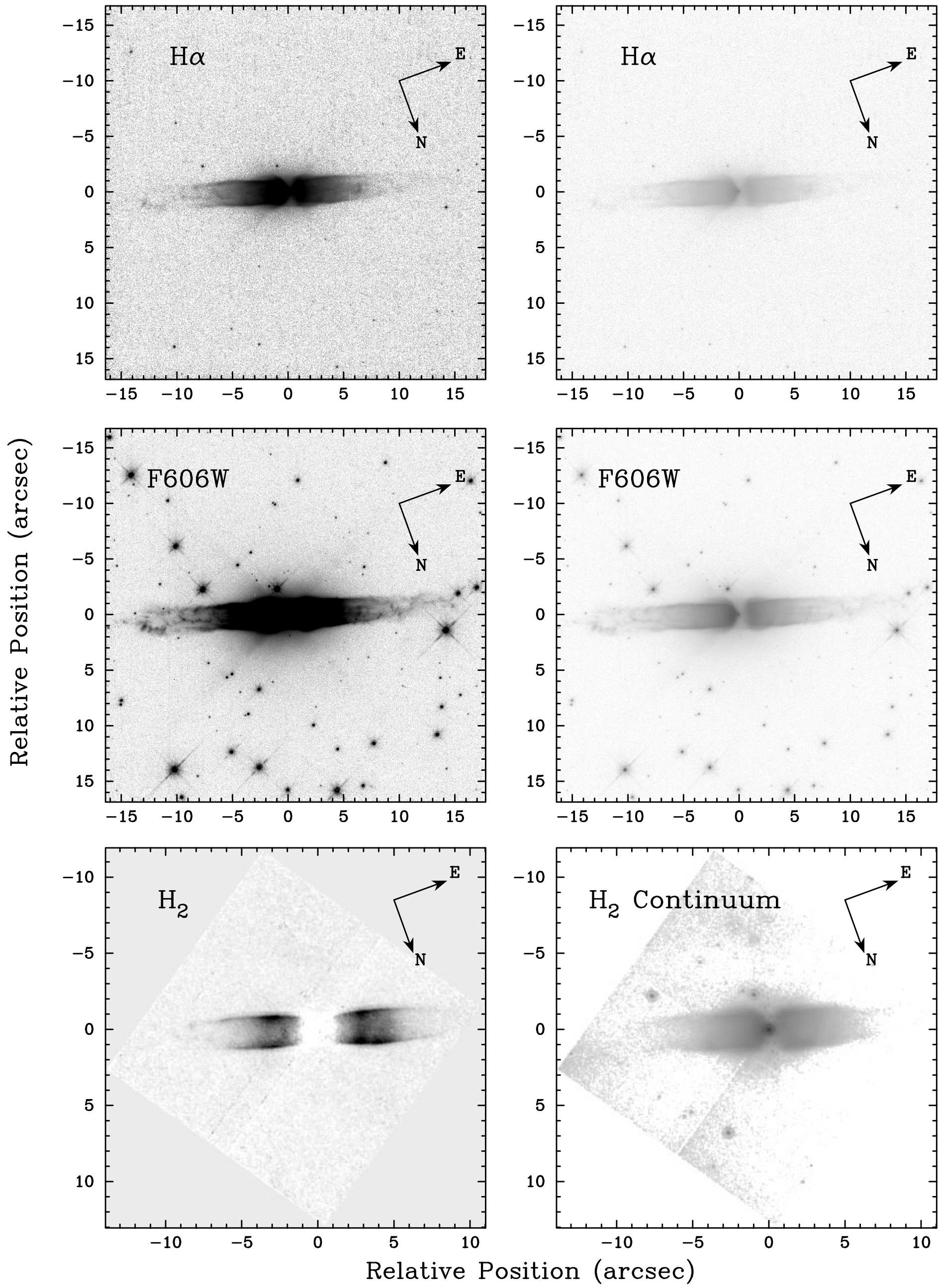

FIG. 1.—Logarithmic-scale *HST* images of Hen 401 obtained in the light of Hα (*top*) and the broad WFPC2 F606W filter (*middle*). The images are displayed with two different contrast levels in order to show both the faint outer emission (*left*) and the bright central inner region (*right*). The bottom panel also shows the H_2 continuum-subtracted image of Hen 401 at $\lambda 2.122$ μm (*left*), together with the image containing the emission in the adjacent continuum at 2.15 μm (*right*). Both images are also displayed in logarithmic scale.

identification is uncertain. When possible, line identifications have been tested by comparing empirical and theoretical line ratios. In Table 1, the absolute integrated fluxes, normalized to $H\beta = 100$, are not corrected for reddening, and they correspond to the spectrum taken in 1995. The mean absolute Hβ flux not corrected for extinction was found to be 5.7×10^{-13} ergs cm^{-2} s^{-1}. Associated errors are in the range of 10%–50%, depending on the strength of the line.

4. DATA ANALYSIS

4.1. *Reddening*

A first approximation to the reddening correction to be applied to the emission-line flux ratios observed can be obtained from an analysis of the H I Balmer decrement. Assuming case B recombination theory and a standard interstellar reddening law, we obtain a value of $E(B-V) = 1.3 \pm 0.4$, which implies a visual extinction of 4.0 ± 1.0 mag. This strong reddening would explain the red slope observed in spite of the fact that the central star is assumed to be of B type.

Deviations from case B predictions, however, are expected in high-density regions, where self-absorption effects and collisional excitation can be important. There are reasons to suspect, as we discuss below, that most of the emission lines we observe in Hen 401 are formed in a very high density environment. Even taking into account these effects, and following Köppen et al. (1982), we estimate that

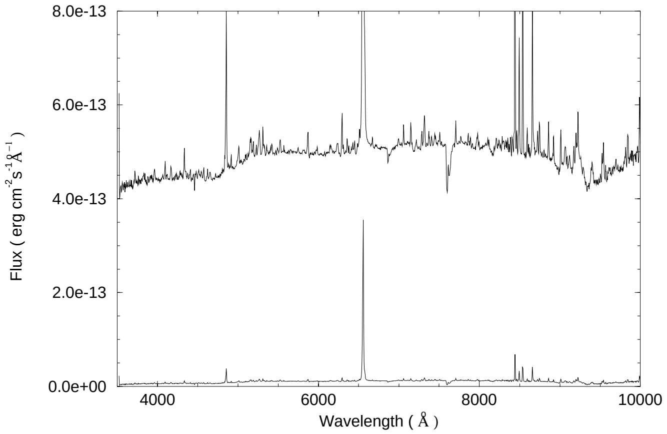

FIG. 2.—Low-resolution optical spectrum of Hen 401. The ordinate scale corresponds to the lower spectrum. The upper spectrum is the result of expanding the lower one by a factor of 10. It is displayed shifted to show the weaker features.

for a stellar temperature of 20,000 K, a dilution factor of 10^{-2} and a moderate self-absorption with $\tau(\mathrm{H}\alpha) = 3.7$, $E(B-V)$ would be ~ 1.6, still compatible with the value derived above and with the extremely reddened shape of the continuum observed. Thus, we will adopt $E(B-V) = 1.3$ for the following calculations.

4.2. *Physical Parameters*

The electron density has been derived from analysis of several emission-line intensity ratios. The dereddened [N II] λ6584/5755 ratio of 11.6 suggests that the emission originates in a high-density gas. Adopting an electron temperature of 10,000 K, this ratio implies a density of $\sim 2 \times 10^5$ cm^{-3}; lower densities would correspond to higher temperatures (i.e., 4×10^4 cm^{-3} for $T_e = 20{,}000$ K). Smaller values of the electron density would imply unrealistically high electron temperatures.

The large [S II] (λ4068 + λ4076)/(λ6717 + λ6731) ratio also corresponds to a high-density regime, where its value is weakly dependent on the temperature, and can also be used to estimate the electron density in Hen 401. From the observed ratio of 8.1, a value of $n_e \simeq 2 \times 10^5$ cm^{-3} is again derived [$n_e = (1.6\text{–}2.3) \times 10^5$ cm^{-3} for $T_e = (2\text{–}1) \times 10^4$ K].

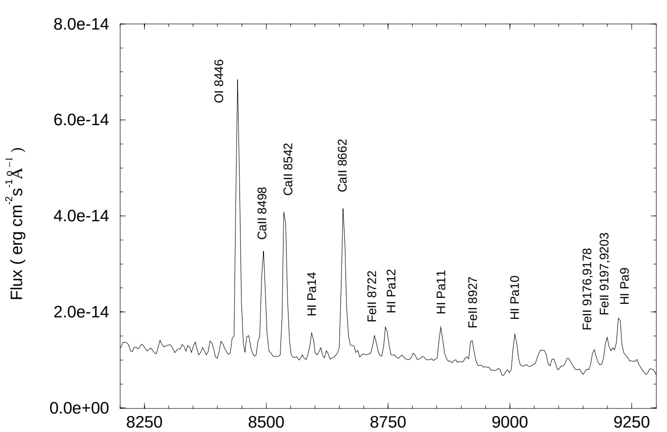

FIG. 3.—Section of the low-resolution optical spectrum of Hen 401 showing the strong O I emission at λ8446 Å and the Ca II infrared triplet.

In contrast, using the standard [S II] λ6717/λ6731 doublet ratio to estimate the density, we obtain a much lower value of only 700 ± 100 cm^{-3}. This value cannot be reconciled with the much higher densities derived above, and implies that the auroral forbidden emission lines are formed in a region of much higher density, where the nebular lines are collisionally deexcited.

4.3. *Fluorescence Excitation*

Among the permitted lines, the O I 8446 Å emission is the strongest feature observed in Hen 401, apart from Hα. Several other permitted O I emission lines are detected in our spectra and identified in Table 1 as due to O I at 7002, 7254, 7774, and 7990 Å. From an analysis of the relative intensities of the O I lines and the dereddened O I λ8446/Hα ratio, we conclude that Lyβ fluorescence, combined with continuum fluorescence (direct excitation by radiation coming from the central star), are needed to explain the values observed, while recombination and collisional excitation effects do not seem to be important.

4.4. *A High-Density Contrast*

The detection of the strong infrared Ca II triplet at 8498, 8542, and 8662 Å, and the [Ca II] lines at 7290 and 7324 Å, supports the presence of a dense, warm neutral region of a very high density in the core of Hen 401, where Ca is singly ionized and H is predominantly neutral.

At these high densities, the resonance Ca II H and K lines become optically thick, enhancing the triplet emission. The Ca II/[Ca II] ratio sets important limits to the density and optical depth of the emitting region. Following the calculations made by Ferland & Persson (1989), we derive a density in excess of 10^9 cm^{-3}, but not higher than 10^{10} cm^{-3}, since the [Ca II] emission lines would then be collisionally deexcited.

The next constraint is imposed by the fact that the Ca II infrared triplet is optically thick, as deduced from the internal line ratios observed (λ8542/λ8498 = 1.38; λ8662/λ8498 = 1.27). Following Persson, McGregor, & Campbell (1988), we derive a lower limit of 30 to the optical depth in the Ca II emitting region at 8542 Å.

The rich iron spectrum observed is also consistent with the presence of a high-density contrast in the inner core of Hen 401. This is concluded from the simultaneous detection of several multiplets of permitted and forbidden singly ionized iron identified in the spectrum and listed in Table 1.

The permitted Fe II lines arising from upper states with energies above 11.3 eV, such as those at 8926, 9177, and 9203 Å, can be originated by Lyα fluorescence (see Hammann & Simon 1988 for a discussion of the mechanism of excitation of these lines in MWC 349A, which displays a very similar Fe II spectrum). Those corresponding to upper levels between 5 and 7 eV, most of them in the ranges 4180–4600 Å, 4900–5400 Å, and 6300–6500 Å, and the individual lines at 7711, 7866, and 9997 Å, can be excited by collisions from lower levels, radiative decays from upper levels, or continuum fluorescence. All these emission lines are optically thick, as is evident from the relative intensities of lines belonging to the same multiplet, suggesting that they are formed in a very high density environment, which might be the same region in which the infrared Ca II triplet lines are formed.

On the other hand, the forbidden [Fe II] emission lines would be collisionally deexcited in regions where electron

TABLE 1

EMISSION LINES IDENTIFIED IN THE OPTICAL SPECTRUM OF HEN 401

λ (Å)	Identification	I (Hβ = 100)[a]
3722	[O II] (1F) 3726.0, 3728.8	7.1
3884	He I (2) 3888.6, H_8 3889.1	3.4
3965	H_ϵ 3970.1	9.5
4070	[S II] (1F) 4068.6, 4076.3	3.0
4108	Hδ 4101.7	10.4
4123+4129	Fe II (28) 4122.6, (27) 4128.7, Si II (3) 4128.1	4.8
4178	[Fe II] (21F) 4177.2, Fe II (27) 4173.5, (28) 4178.9	10.6
4234	Fe II (27) 4233.2, [Fe II] (21F) 4231.5	2.5
4245	[Fe II] (21F) 4244.0, 4244.8	2.8
4278	[Fe II] (21F) 4276.8, Fe II (27) 4273.3, (32) 4278.1	1.4
4287	[Fe II] (7F) 4287.4	4.2
4294	Fe II (28) 4296.6	1.8
4304	Fe II (27) 4303.2, [Fe II] (21F) 4305.9	d
4323	[Fe II] (21F) 4319.6	d
4342	Hγ 4340.5, [Fe II] (21F) 4346.8	22.2
4353+4360	[Fe II] (21F) 4346.8, (7F) 4359.3, 4352.8, 4358.4, Fe II (27) 4351.8	d
4387	Fe II (27) 4385.4, (32) 4384.3	2.7
4417	[Fe II] (6F) 4414.5, 4416.3, (7F) 4413.8, Fe II (27) 4416.8	5.4
4456	[Fe II] (7F) 4452.1, (6F) 4457.9	d
4521	Fe II (37) 4515.3, 4520.2, (38) 4522.6	4.3
4555	Fe II (37) (38) 4555.9, 4549.5	4.5
4584	Fe II (38) 4582.8, 4583.8	5.7
4631	Fe II (37) 4629.3	3.7
4659+4664	Fe II (43) 4657.0, (44) 4663.7, (37) 4666.8, [Fe II] (4F) 4664.4	5.9
4703+4715	[Fe III] (3F) 4701.3, He I (12) 4713.1, 4713.4	1.8
4732	[Fe II] (4F) 4728.1, (3F) 4729.8, Fe II (43) 4731.4, [Fe III] (3F) 4733.9	d
4816	[Fe II] (20F) 4814.5	2.0
4863	Hβ 4861.3	100.0
4926	Fe II (42) 4923.9	7.0
4995	Fe II (36) 4993.8	6.2
5008+5020	Fe II (42) 5018.4, [Fe II] (20F) 5005.5, 5020.2	17.4
5101	Fe II (35) 5100.7	2.5
5109	[Fe II] (18F) 5108.0, (19F) 5111.6	2.5
5134	Fe II (35) 5132.7, 5136.8	1.4
5160	[Fe II] (18F) 5158.0, (19F) 5158.8, (35F) 5163.9, Fe II (35) 5161.2	10.0
5171	Fe II (42) 5169.0, Fe II (35) 5171.6	7.1
5199	Fe II (49) 5197.6	5.8
5237	Fe II (49) 5234.6	5.1
5286	Fe II (41) 5284.1, [Fe II] (16F) 5280.3, (35F) 5283.1	d
5318	Fe II (48) 5316.6, 5316.8	15.0
5328	Fe II (49) 5325.5	1.5
5336	[Fe II] (19F) 5333.6, Fe II (48) 5337.7	5.9
5365	Fe II (48) 5362.9	4.4
5377	[Fe II] (19F) 5376.5	2.2
5413	[Fe II] (16F) 5413.3, (17F) 5412.6, Fe II (48) 5414.1	3.3
5426+5435	[Fe II] (18F) 5433.0, Fe II (49) 5425.3	6.9
5478	[Fe II] (34F) 5477.25	2.1
5500+5507	[Fe II] (17F) 5495.8, [Fe II] 5006.0	4.3
5529+5536	[Fe II] (17F) 5527.3, (34F) 5527.6, Fe II (55) 5534.9	12.3
5746+5756	[Fe II] (34F) 5747.0, [N II] (3F) 5754.8	3.9
5877	He I (11) 5875.7	14.5
5979	Si II (4) 5979.0	2.5
5992	Fe II (46) 5191.4, O I (44) 5991–5995	4.0
6084+6129	Fe II (46) 6084.1, 6113.3, 6129.7	d
6149	Fe II (74) 6147.7, 6149.2	d
6239	Fe II (74) 6238.4, 6239.9	12.1
6249	Fe II (74) 6247.6, Fe II 6247.6	d
6300	[O I] (1F) 6300.2	24.0
6317	Fe II 6318.0	5.5
6347	Si II (2) 6347.1	d
6365	[O I] (1F) 6363.9, Si II (2) 6371.4, [Ni II] (8F) 6365.5	10.6
6384	Fe II 6383.7, 6385.5	3.1
6417	Fe II (74) 6416.9	3.5

TABLE 1—*Continued*

λ (Å)	Identification	I (Hβ = 100)[a]
6427	Fe II (40) 6432.6	8.9
6456	Fe II (74) 6456.4	9.9
6493	Fe II 6491.2, 6493.0	4.8
6516	Fe II (40) 6516.1	8.2
6563	Hα 6562.8, [N II] (1F) 6548.1	1318.0
6581	[N II] (1F) 6583.6	61.2
6667	[Ni II] (2F) 6668.1	1.4
6678	He I (46) 6678.1	5.0
6717	[S II] (2F) 6716.4	1.8
6731	[S II] (2F) 6730.8	1.8
7001	[Fe II] (15F) 7005, O I (21) 7002.1	6.1
7067	He I (10) 7065.3	10.9
7156	[Fe II] (14F) 7155.1	11.1
7257	[Ni II] (7F) 7256, O I (20) 7254.4	d
7284	[Ca II] 7291.5, He I (45) 7281.3, Fe II (72) 7289	7.5
7320	[Ca II] (1F) 7323.9, [O II] (2F) 7320–7330	28.0
7375+7385	[Ni II] (2F) 7377.8, [Fe II] (14F) 7388.2	6.5+4.9
7412	[Ni II] (2F) 7411.6	6.7
7452+7464	[Fe II] (14F) 7452.5, Fe II (73) 7462.6	7.7+3.7
7492+7508	Fe II 7495.6, Fe II (73) 7515.3	4.6+8.5
7528	Fe II 7533.4	2.3
7706	Fe II 7711.4, Fe II 7711.7	10.8
7770	O I (1) 7774	5.7
7861	Fe II 7866.5	5.3
7874	Mg II (8) 7877.1	1.4
7898	Mg II (8) 7896.4	3.6
7912	Fe II 7917.8	2.6
7968	Fe II 7969.0,7970.4, Fe II 7969.0	5.7
7979	Fe II 7975.6, Fe II 7981.9	8.4
7994	O I 7990.0, [Fe II] (1F) 7999.5	2.9
8123	Mg II 8115.2, 8120.4	d
8217	Mg II 8214.0	9.7
8234	Mg II 8233.2, 8234.6	2.7
8245	Fe II 8250.4	4.7
8286	Fe II 8287.6, 8287.9	23.6
8306	Fe II 8305.7, [Ni II] (2F) 8303.3	22.1
8355	Fe II 8352.8, Fe II 8357.2	4.0
8428	Fe II 8423.9	d
8445	O I (4) 8446, H I Pa18 8438.0, Fe II 8450.8	161.5
8462	H I Pa17 8467.3, Fe II 8468.1	14.2
8492	Ca II (2) 8498.0, H I Pa16 8502.5, Fe II 8490.9	71.5
8538	Ca II (2) 8542.1, H I Pa15 8545.4	93.0
8594	H I Pa14 8598.4	15.5
8617	[Fe II] (13F) 8617.0	d
8661	Ca II (2) 8662.1, H I Pa13 8665.0	95.5
8722	Fe II 8722.4	13.0
8746	H I Pa12 8750.5	19.0
8802	Fe II 8806.2	d
8858	H I Pa11 8862.8	20.8
8895	[Fe II] (13F) 8891.9	d
8922	Fe II 8926.7	13.6
9011	H I Pa10 9014.9	18.9
9066	C I (3) 9061.5, 9062.5	20.7
9088	C I (3) 9088.4	4.2
9119	Fe II 9122.9	8.0
9172	Fe II 9175.8, 9178.0	10.2
9200	Fe II 9196.9, Fe II 9203.1	17.0
9229	H I Pa9 9229.0, Mg II (1) 9218.2	33.0
9247	Mg II (1) 9244.3, Fe II 9251.7	d
9524	Fe II 9526.8	12.8
9540	H I Pa10 9546.0	27.9
9990	Fe II 9997.6	45.7
10041	H I Pa7 10049.4	83.6

[a] d: detected, but very faint.

densities exceed a critical value. Thus, we estimate that the [Fe II] spectrum should arise in regions with $n_e \leq 10^6$ cm^{-3}.

5. DISCUSSION

Altogether, our results confirm the identification of Hen 401 as a new bipolar reflection nebula in the proto-PN stage. The bipolar morphology, as well as the other physical properties derived above, are very similar to those found in other well-known proto-PNs and young PNs, such as CRL 2688, M1-92, M2-9, or the recently discovered IRAS 17150−3224 and IRAS 17423−1755.

The overall morphology of Hen 401 as revealed by the *HST* images is remarkably similar to that of M2-9 (Balick, Icke, & Mellema 1997; Schwartz et al. 1997), while the optical spectrum of Hen 401 closely resembles the spectrum of M1-92 (Trammell, Dinnerstein, & Goodrich 1993; Solf 1994), with strong Balmer emission and a combination of permitted and forbidden emission lines of iron and other atomic elements superimposed on a red continuum.

A very steep density gradient must be invoked to explain the simultaneous detection of spectral lines formed under very different density conditions (from 1000 cm^{-3} up to 10^9 cm^{-3}). As suggested by the available polarization data (Scarrot & Scarrot 1995), the emission observed in Hen 401 could naturally be explained by the presence of a dense circumstellar disk, which would be responsible for the strong collimation of the outflow and for the dark lane observed in between the two main lobes.

The same scenario has been proposed to explain the overall morphology and the spectrum of M1-92 (Trammell et al. 1993), where the continuum emission and part of the permitted emission observed is interpreted as light reflected by dust scattering in the lobes, while the forbidden line emission and the remainder permitted emission would be produced locally and probably due to shocks (Solf 1994).

Shocked knots of material in the light of [S II] and [O I] have been found along the bipolar axis of many of these bipolar proto-PNs and young PNs, such as M1-92 itself (Bujarrabal et al. 1998) or IRAS 17423−1755, for which ground-based spectroscopy also revealed a strong emission in the light of [S II], [N II] and [O I] (Riera et al. 1995), with ratios consistent with shock excitation.

In the case of Hen 401, an inspection of the *HST* images taken in different filters, as we have already mentioned, does not reveal significant morphological differences. Thus, the extended emission observed must be mostly due to dust scattering and not to intrinsic photoionization of the bipolar lobes. Sahai et al. (1999) reports the tentative detection of two small shock-emitting blobs located along the nebular axis about 6″.2 from the central star at a 3–5 σ level. However, this cannot be confirmed by our two-dimensional spectroscopy, where no variations are found between the spectrum of the central regions and that of the lobes.

The strong near-infrared excess reported in García-Lario et al. (1997) and the broad Balmer lines detected in the spectra of Hen 401 suggest that mass loss might still be active. Similar non-Gaussian profiles with extended wings in the Balmer lines, which in the case of Hα extend up to 1600 km s^{-1} with respect to the velocity of the emission peak in Hen 401, have also been observed in other proto-PNs and young PNs. M2-9 shows velocities in excess of 1200 km s^{-1} (Torres-Peimbert & Arrieta 1998), and the spectacular IRAS 17423−1755 displays a wide Hα profile with a redward edge shifted 1090 km s^{-1} (Riera et al. 1995). In all cases, the broad profiles found are interpreted as indicating mass outflows.

The detection of H_2 emission in another bipolar proto-PN where photoionization has not yet taken place confirms the results previously obtained by Weintraub et al. (1998). They suggest that H_2 emission occurs at an intermediate stage after the generation of the bipolar structure and before photoionization transforms a proto-PN into a PN.

With the available information, however, it is difficult to determine whether the origin of the H_2 emission observed lies in continuum fluorescence or shocks induced by high-velocity outflowing material. In a recent study of a sample of bipolar PNs showing H_2 emission carried out by Guerrero et al. (1999), it was found that very young PNs are usually dominated by Brγ emission, while more evolved PNs show very strong H_2 emission at 2.122 μm, sometimes much stronger than Brγ. Fluorescence seems to be the main mechanism that excites molecular hydrogen in the high-density inner regions of the youngest PNs. In contrast, this emission is found to be concentrated in the walls of the lobes and in the ring of gas collimating the outflow in highly evolved PNs, where it is interpreted as shock-excited emission.

Additional spectroscopic measurements of other diagnostic H_2 lines would be needed to unambiguously establish the nature of the emission observed in Hen 401 by comparing the line ratios observed with excitation models. The detection in the optical spectrum of other emission lines that probably originate from continuum fluorescence, together with the apparent lack of shock-excited optical emission in the lobes, makes the fluorescence option more attractive a priori. However, as we have seen, shock-excited H_2 emission is expected to be concentrated in the walls of the lobes, as is observed in the case of Hen 401.

6. CONCLUSIONS

Based on a combination of ground-based optical and near-infrared spectroscopy with optical and near-infrared *HST* images, we confirm the identification of Hen 401 as a bipolar proto-PN surrounded by a highly elongated nebula.

Consistent with what has previously been reported in the case of some other well-known bipolar proto-PNs and young PNs, emission lines formed under very different density conditions are detected in the optical spectrum of Hen 401, indicating that a high-density contrast must exist very close to the central star. This, together with the strong obscuration observed in the waist between the main bipolar lobes, strongly suggests the presence of a thick circumstellar disk, which might be responsible for the collimation of the outflow observed.

The strong near-infrared excess found associated with Hen 401 and the broad Hα profile detected in our spectra indicate that mass loss might still be active.

From the similar morphology at all wavelengths and from our optical spectroscopy, we conclude that the emission observed is mainly scattered light, probably originating in the fluorescence-excited inner region of the circumstellar disk, and not intrinsic photoionization or shock-excited emission.

However, strong molecular hydrogen emission is also detected in Hen 401, concentrated in the walls of the lobes, an effect that is usually attributed to shocks. Unfortunately, with the available information, it is not yet possible to determine whether the origin of the H_2 emission observed is continuum fluorescence or shocks induced by high-velocity outflowing material.

Finally, our results confirm that the onset of the H_2 emission occurs in proto-PNs after the bipolar structure has developed, but before photoionization takes place.

This work was funded through grants PB94-1274 and PB97-1435-C02-02 from the Spanish Dirección General de Investigación Científica y Técnica (DGICYT). A. R. acknowledges partial financial support through grant PB95-0066 from the Spanish DGICYT. We thank Gail Conway for her contribution to the IRSPEC data reduction.

REFERENCES

Allen, D. A. 1978, MNRAS, 184, 601
Allen, D. A., & Glass, I. S. 1975, MNRAS, 170, 579
Balick, B., Icke, V., & Mellema, G. 1997, Hubble Catches Up with a Blue Straggler Star (STScI press release STScI-PR97-35)
Bujarrabal, V., Alcolea, J., Sahai, R., Zamorano, J., & Zijlstra, A. A. 1998, A&A, 331, 361
Bujarrabal, V., & Bachiller, R. 1991, A&A, 242, 247
Ferland, G. J., & Persson, S. E. 1989, ApJ, 347, 656
García-Lario, P., Manchado, A., Pych, W., & Pottasch, S. R. 1997, A&AS, 126, 479
Hammann, F., & Simon, M. 1988, ApJ, 327, 876
Guerrero, M., Villaver, E., Manchado, A., García-Lario, P., & Cernicharo, J. 1999, ApJ, submitted
Köppen, J., Finkenzeller, U., Mundt, R., & Beltrametti, M. 1982, A&A, 112, 174
Loup, C., Forveille, T., Nyman, L. A., & Omont, A. 1990, A&A, 227, L29
Moore, C. E. 1972, A Multiplet Table of Astrophysical Interest (Washington: National Bureau of Standards)
Parthasarathy, M., & Pottasch, S. R. 1989, A&A, 225, 521
Persson, S. E., McGregor, P. J., & Campbell, B. 1988, ApJ, 326, 339
Riera, A., García-Lario, P., Manchado, A., Raga, A., & Pottasch, S. R. 1995, A&A, 302, 137
Sahai, R., Bujarrabal, V., & Zijlstra, A. 1999, ApJ, 518, L115
Sanduleak, N., & Stephenson, C. B. 1973, ApJ, 185, 899
Scarrot, S. M., & Scarrot, R. M. J. 1995, MNRAS, 277, 277
Schwartz, H. E., Aspin, C., Corradi, R. L. M., & Reipurth, B. 1997, A&A, 319, 267
Silva, A. M., Azcárate, I. N., Poppel, W. G. L., & Likkel, L. 1993, A&A, 275, 510
Solf, J. 1994, A&A, 282, 567
Stephenson, C. B. 1971, Publ. Warner & Swasey Obs., 1(4), 4
Torres-Peimbert, S., & Arrieta, A. 1998, Rev. Mexicana Astron. Atrofis., 7, 171
Trammell, S. R., Dinnerstein, H. L., & Goodrich, R. W. 1993, ApJ, 402, 249
Weintraub, D. A., Huard, T., Kastner, J., & Gatley, I. 1998, ApJ, 509, 728